AUTHOR(S):

NAKAO, Yukiko; SUGIMURA, Kazuki; NISHIO, Yoshiyuki

京都大学学術情報リポジトリ
KURENAI 紅
Kyoto University Research Information Repository

CaCO$_3$ mineralization in polymer composites with cellulose nanocrystals providing a chiral nematic mesomorphic structure

Yukiko Nakao, Kazuki Sugimura*, and Yoshiyuki Nishio

Division of Forest and Biomaterials Science, Graduate School of Agriculture, Kyoto University, Sakyo-ku, Kyoto 606-8502, Japan

*To whom correspondence should be addressed.

E-mail: kazusugi@kais.kyoto-u.ac.jp.   Phone: +81 75 753 6252.   Fax: +81 75 753 6300.

1. Introduction

Cellulose nanocrystals (CNCs) are highly crystalline rod-like particles typically with 100–200 nm lengths and 5–10 nm widths, conventionally obtained by sulfuric acid-hydrolysis of native cellulose fibers (e.g., cotton or wood pulp) [1–5]. In water, the CNC particles are negatively charged by sulfate half-esters on the surfaces and show adequate dispersion, yielding a stable colloidal suspension. Above a critical CNC concentration (3–5 wt% for cotton-derived CNC), the apparently homogeneous suspension phase-separates into an optically isotropic phase (upper) and a birefringent mesophase (lower) in the course of standing of the fluid sample [1,6,7]. The mesogenic arrangement in the colloidal mesophase is usually "chiral nematic" (or "cholesteric" as synonym) [8]; this is also the case for the molecular mesophases of cellulose derivatives [9–12]. The assembly structure is characterized by the director of nematic orientation that propagates rotationally along one direction to make a helical trajectory of pitch P. When the value of P is comparable to wavelengths (λ) of visible light, the formed chiral nematic mesophase imparts a color due to λ-selective light reflection. If P is well over 1 μm, the mesophase can exhibit a fingerprint texture of periodic retardation lines under a polarized optical microscope.

The chiral nematic structure of cellulosics can be made permanent in polymer films or gels [12,13], typically, by polymerization of solvent monomers (such as acrylic monomers [14–16] and alkoxysilanes [17–20]) constituting the cellulosics' lyotropics. Thereby, we can expand the variety of cellulose-based solid materials that excel in a specific functionality and/or mechanical performance. With regard to the use of CNC liquid crystals, for example, MacLachlan, Hamad, and their coworkers synthesized iridescently colored CNC–silica composites and mesoporous silicas from chiral nematic CNC/alkoxysilane lyotropics, aiming for the development of photonic and electronic materials [21,22]. To give another example using CNCs as mesofiller, Tatsumi et al. demonstrated successful fabrication of unique polymer composites reinforced by locking-in the ordered CNC assembly that was formed in an aqueous methacrylate monomer solution [23,24]; the composites showed definite mechanical anisotropy, when the parent CNC lyotropics were oriented under a specific magnetic field before the locking-in process via polymerization of the monomer.

Calcic mineralization in cellulosics-derived chiral nematic layered matrices can also be an interesting

assignment to develop a new class of cellulosic composites [12,25]. This route may be categorized into the "biomimetic" design and fabrication of advanced organic–inorganic hybrid materials [26–30]. In actuality, many natural organisms possess an ability to mineralize calcic ingredients under mild aqueous surrounding conditions in association with variously structured polypeptides and/or polysaccharides as templates [31–34]. In this context, first, the author's group studied a calcium phosphate mineralization using liquid-crystalline gels of ethyl cellulose (EC)/poly(acrylic acid) (PAA) and hydroxypropyl cellulose (HPC)/PAA [25]; the binary polymer samples were prepared in colored film form from EC and HPC lyotropics of left-handed and right-handed chiral nematics, respectively, by polymerization and cross-linking of the solvent, acrylic acid (AA). The mineralization was performed in a batchwise process by soaking of the films in an aqueous salt solution containing the relevant ions, Ca^{2+} and HPO_4^{2-}, under a weak-basic condition, so that the ions were efficiently taken in the swollen films as a quasi-Donnan membrane. As a result, we successfully obtained $Ca_3(PO_4)_2$ (or hydroxyapatite)-incorporated EC/PAA and HPC/PAA composites, which retained the chiral nematic supramolecular structure of the respective original handedness and displayed reflective colorations. In a second study [35], we conducted calcium carbonate ($CaCO_3$) mineralization again using the chiral mesomorphic EC/PAA films and successfully gained a series of colorful mineralized films functioning as a chiroptical hard medium. Actually, this kind of inorganic hybridization remarkably improved the thermomechanical performance of the pristine polymer films. Another notice in the second example was the observation that calcite, aragonite, and amorphous $CaCO_3$ were each individually deposited inside the EC/PAA films by immersion in a salted water providing Ca^{2+}, HCO_3^-, and additional Mg^{2+}, the selectivity of $CaCO_3$ polymorph depending on the ionic conditions of pH and Mg/Ca proportion.

Against the background stated above, the present paper deals with $CaCO_3$ mineralization using CNC/vinyl polymer composites in which the CNC chiral mesomorphic structure (habitually left-handed [12,36]) is stabilized with the synthetic polymer. Nonionic poly(2-hydroxyethyl methacrylate) (PHEMA) and partly anionic poly(2-hydroxyethyl methacrylate-*co*-acrylic acid) (P(HEMA-*co*-AA)) are employed as the polymer component capable of forming a hydrogel. The AA-containing copolymer has carboxylic acid groups (which may bind Ca^{2+})

3

and can be a good provider of the substantial scaffolding sites for inorganic deposition. The mesogenic constituent CNC has sulfate groups ($-OSO_3^-$) on the surface, possibly, being another effective scaffold for the nucleation and growth of the calcic biomineral. In relation to such interactive situations, herein, we focused on the $CaCO_3$ polymorphs occurring in the mineralized CNC/polymer composites, the starting film samples being prepared with various compositions involving the CNC concentration and HEMA:AA ratio. Attention was also directed to some aftereffects of the mineralization on the matrix properties, specifically, to the change in the chiral nematic pitch and the improvement in thermal resistance of the ordered CNC/polymer films.

2. Experimental

2.1. Original materials

Cotton-derived fibrous cellulose was obtained by cutting and milling of Whatman filter paper No. 5 (GE Healthcare Life Sciences Corp.). Sulfuric acid (Nacalai Tesque, Inc.) and polyethylene glycol (PEG; molecular weight = ~20,000, Wako Pure Chemical Ind., Ltd.) were used as received. Monomers, HEMA (Wako Pure Chemical Ind., Ltd.) and AA (Nacalai Tesque, Inc.), were purified by vacuum distillation before use. A photopolymerization initiator, 2-hydroxy-2-methylpropiophenone (HMPPh; Sigma-Aldrich), and a cross-linking agent, ethylene dimethacrylate (EDM; Tokyo Kasei Kogyo Co., Ltd.), were used without further purification. Calcium chloride dihydrate ($CaCl_2 \cdot 2H_2O$) and ammonium carbonate ((NH_4)$_2CO_3$) were purchased from Nacalai Tesque, Inc. and used as ion sources for mineralization. A low-molecular-weight PAA (L-PAA; average degree of polymerization (DP) = 25, Sigma-Aldrich) was used as a precipitation inhibitor in the salt solution of ion server [25,37]. Other conventional chemicals were purchased from Wako Pure Chemical Ind., Ltd. or Nacalai Tesque, Inc. and used as received.

2.2. Preparation of CNC/aqueous monomer suspensions

CNCs were isolated from the powdered cellulose (Whatman, No. 5) by acid hydrolysis with 65 wt% sulfuric acid, with mechanical stirring at 70 °C for 15 min [7]. After a dilution and centrifugation process, the crude CNC

dispersion was dialyzed in distilled water and then in 7 wt% PEG aqueous solution. Ultimately, a refined CNC/water suspension was prepared at 23 wt% via finishing treatment using a homogenizer. The particle dimensions of CNC were ~110 nm in length and ~8 nm in diameter on average, when estimated by transmission electron microscopy. Surface sulfur content of the CNC particles approximated 0.65 wt%, when determined by an alkali titration method [7].

The preparation of CNC suspensions in aqueous monomer (HEMA/water or HEMA/AA/water) was done by reference to a procedure described in an earlier paper [23]. Briefly, a weighed amount of the concentrated CNC/water suspension mentioned above was mixed with HEMA or HEMA/AA (95:5–70:30 in mol) and distilled water (diluent) in a light-blocked glass vial, using ultrasonic-wave treatment for 2 min. The weight ratio of monomer/water was adjusted to 1:1, and HMPPh and EDM were fed in the solvent, each at 0.5 wt%. 7–11 wt% CNC/monomer/water suspensions were thus prepared and stored at room temperature (25 °C) usually in a dark place.

2.3. Preparation of CNC/polymer composite films

The CNC suspensions in monomer/water (1:1 in wt) were allowed to stand in the dark quiescently for 1 week. Most samples of CNC = 7 and 9 wt% separated into isotropic (upper) and anisotropic (lower) phases in a glass container, but 11 wt% CNC suspensions were totally anisotropic. An adequate quantity (~2.8 g) of the respective anisotropic parts, pipetted off from the parent suspensions, was poured into a Teflon-coated dish ($\phi = 50$ mm) and irradiated with UV light of ~350 nm for 2 h. For this irradiation to polymerize the solvent monomer, a large UV lamp, 10 W FL10BLB-A (Toshiba Lightning & Technology Corp.) was used, and the sample was placed at a distance of ~5 cm from the light source in an atmosphere of N_2 gas. After the polymerization process, the almost solidified product (CNC/PHEMA or CNC/P(HEMA-*co*-AA)) was oven-cured at 80 °C for ~1 h under an N_2 flow. The CNC/polymer composite films thus obtained were washed with CCl_4 to extract a trace amount of monomer, then vacuum-dried at 40 °C overnight, and finally kept in a desiccator until used. As reference samples, PHEMA and P(HEMA-*co*-AA) films were prepared in a similar procedure from aqueous monomer solutions containing no

CNCs.

For convenience, a code xCNC/PHEMA denotes the composite film obtained from an x wt% CNC suspension in HEMA/water (1:1). When a mixture of HEMA/AA (y : (100−y) in mol) is employed for the starting monomer, the produced film is encoded as xCNC/P(HEMA$_y$-co-AA$_{(100-y)}$). As regards the CNC content in the solid composites, we can roughly estimate the weight percentage, as follows: 20 wt% for $x = 11$, and a little more than 13 and 16.5 wt% for $x = 7$ and 9, respectively.

2.4. Mineralization treatment of CNC/polymer composites

For both the CNC/HEMA and CNC/P(HEMA-co-AA) series, strips 10×10 mm^2 cut from their respective as-prepared larger films were used for mineralization experiments. A large quantity of salt solution containing 10 mM CaCl$_2$, 10 mM (NH$_4$)$_2$CO$_3$, and 0.5 mM L-PAA in the monomer unit was prepared at 25 °C and at pH = 9.0 (adjusted using NaOH/HCl aq.). Each strip was immersed in 100 mL of the salt solution and the system whole was thermostated at 30 °C in an incubator for a prescribed period of 1–5 days. The salt solution as ion supplier was exchanged for fresh one at intervals of 24 h. After the mineralization process, the treated strips were rinsed in distilled water for 10 min, then air-dried, and subsequently vacuum-dried at 40 °C.

In what follows, the sample codes, m-xCNC/PHEMA_nd and m-xCNC/P(HEMA$_y$-co-AA$_{(100-y)}$)_nd, are used to represent the composite films mineralized for n days (n = 1–5).

2.5. Measurements

Optical characterization of CNC/aqueous monomer suspensions and CNC/polymer composites was made using a polarized optical microscope (POM), Olympus BX60F5 equipped with a digital camera (DP50-WMED). For observations, the suspensions (anisotropic) were sealed in a glass cell of rectangular shape (ca. 40 mm × 10 mm × 1 mm) and the composite films were put directly on a slide glass.

Fracture surfaces of CNC/polymer composites and their mineralized ones were observed by using a field emission scanning electron microscope (FE-SEM), Hitachi S-4800, after sputter coating with platinum. For the

6

mineralized samples, energy-dispersive X-ray (EDX) analysis was also conducted using an EDAX Genesis XM2 to examine the distribution profiles of elements C, O, S, and Ca in the inside of the inorganic-hybridized films.

Wide-angle X-ray diffraction (WAXD) measurements were made on a Rigaku Ultima IV diffractometer, to examine $CaCO_3$ polymorphs for mineralized CNC/polymer composites. The apparatus was operated at 40 kV and 40 mA, and Ni-filtered CuKα (0.1542 nm) radiation was utilized. The diffraction intensity profiles were collected in a range of $2\theta = 4$–$60°$.

Thermogravimetric analysis (TGA) was carried out for 20 mg of film fragments by using a Shimadzu TGA-51 apparatus in an atmosphere of N_2-gas flow. Each sample (vacuum-dried at 100 °C in advance) was heated from 30 to 700 °C at a rate of 5 °C min^{-1}.

When mineralized samples were subjected to the TGA, WAXD, and EDX measurements, the film surfaces were usually polished with a sheet of sandpaper (#2000; grain size < 20 μm) in order to remove a possible contribution of surface-deposited minerals.

3. Results and discussion

3.1. Confirmation of mesomorphic order fixed into CNC/polymer composites

CNC/polymer composites were successfully obtained in a form of optically clear film by polymerization of the monomer solvent (HEMA or HEMA/AA) constituting the precursory anisotropic aqueous CNC suspensions. The visual appearance of as-prepared films is exemplified in Fig. 1a for 9CNC/P(HEMA$_{90}$-co-AA$_{10}$); the slightly yellowish color is derived from the photoinitiator HMPPh. Fig. 1b shows a POM photograph of the composite film. The optical image imparts a well-developed fingerprint pattern made up of periodic retardation lines, which evidences fixation of a chiral nematic structure into the film. The repeating distance S_r of the retardation lines is usually taken as corresponding to half the chiral nematic pitch, i.e., $S_r = P/2$. For the 9CNC/P(HEMA$_{90}$-co-AA$_{10}$) film, P was estimated to be 7.61 μm as an average of the measurements using several areas of the fingerprint pattern. The P value was smaller than the corresponding data 10.1 μm observed for the starting suspension (see Supplementary Materials, Fig. S1 (data a)). This decrease in P may be ascribed mainly to the condensation of the

CNC dispersoid due to evaporation of water and partly to a possible shrinkage of the filmy sample in the process of polymerization of the monomer solvent.
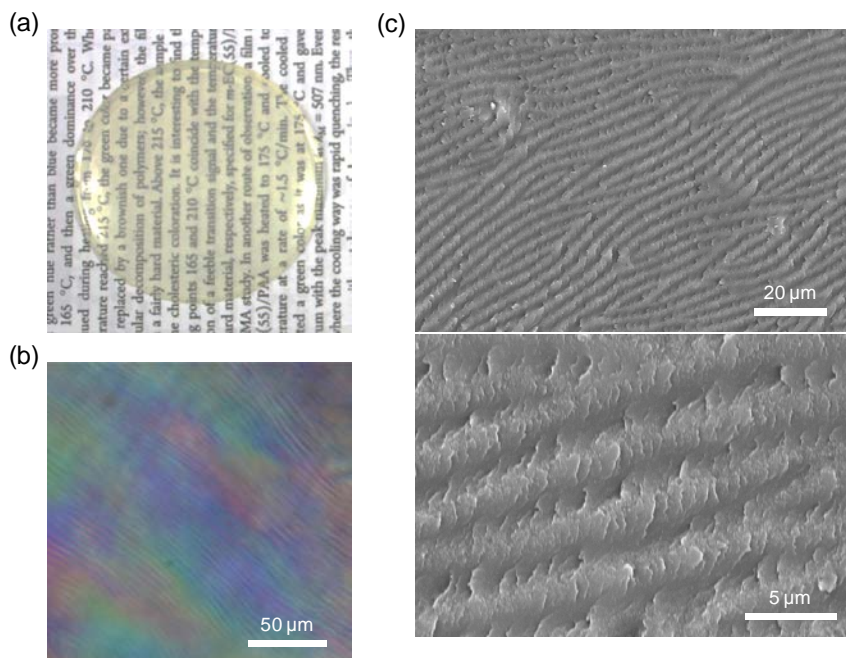

Fig. 1. Visual and microscopic observations for a composite film of 9CNC/P(HEMA$_{90}$-co-AA$_{10}$): (a) visual appearance; (b) POM image; (c) FE-SEM images of the fracture surface (upper, lower magnification; bottom, higher magnification).

Fig. 1c illustrates FE-SEM images observed for the fracture surface of the 9CNC/P(HEMA$_{90}$-co-AA$_{10}$) film. The upper micrograph reveals extensive development of a periodically striated texture corresponding to the optical fingerprint pattern, and the higher magnification (bottom photo) indicates the presence of fibrous entities (assimilation of CNCs) embedded in the polymer matrix. The periodic distance S in the striation texture was estimated using several places in the fracture surface, and $2S = 7.43$ μm was obtained on the average. This value is in good agreement with the data of $2S_r = 7.61$ μm determined as P from the POM image.

Similar morphological observations by POM and FE-SEM were made for many samples which included xCNC/PHEMA and xCNC/P(HEMA$_{90}$-co-AA$_{10}$) with $x = 7$, 9, and 11, and 9CNC/P(HEMA$_y$-co-AA$_{(100-y)}$) with $y = 95$, 90, 80, and 70. It was thus confirmed that the chiral nematic mesomorphic order of CNCs was successfully

8

fixed into all the composite films prepared. However, the observed pitch decreased with increasing CNC concentration (x); this is an accustomed negative correlation between P and the mesogen content. To make another comparison at a given x, the pitch decreased with increasing AA proportion (100−y) (see P data in Table 2 (1st column) shown in *Sec. 3.3.1*). It is well known that the addition of electrolytes (including H$^+$) into CNC aqueous lyotropics leads to decrease of the chiral nematic pitch, to make a negative dependence of P on the ionic strength [6]. A similar electrolytic effect on P was confirmed for the CNC suspensions in HEMA/AA/water used in this study (see POM data in Fig. S1).

## 3.2. Calcic mineralization of CNC/polymer composites

3.2.1. Overview of the process

When film specimens of CNC/polymer composites were soaked in the salt solution for mineralization, they swelled and gradually turned into a translucent gel within 12 h. Even though the swelling was almost equilibrated in 1 day, the optical turbidity of the gelatinous films more or less increased with the passage of immersion time. The swelling degree of CNC/PHEMA films was controlled in a level of 1.15–1.2 times in the sides of the surface square and 1.3–1.4 times in the thickness. As to the CNC/P(HEMA-*co*-AA) series, the films showed a relatively larger expansion of 1.25–1.35 times in the square edge and 1.4–1.9 times in the thickness; the degree increased with an increase in the AA content in the polymer matrix. The CNC component generally served to lower the swelling degree of the matrix, however.

In the course of mineralization for 5 days, the pH of the salt solution at work was measured every 24 h just before the exchange for fresh one. It was confirmed from the monitoring traces that the pH value, initially set at 9.0, was lowered and stabilized at 8.5–8.6 (compared at 25 °C). In the use of the AA-containing copolymer, however, a still lower pH value ($\lesssim$ 8.4) was noted in the first trace, probably due to ionization of the AA unit.

In such a low-basic condition (pH $\leq$ 9) of the salt solution, the ion species taken in the swollen films for mineralization should be Ca^{2+} and HCO$_3^-$. The abundance of the anion species of monovalent form (hydrogen carbonate) at pH $\approx$ 8.4 $\pm$ 0.5 is assured by the established data, pK_{a1} = 6.4 and pK_{a2} = 10.3 [38], for the dissociation

equilibrium of carbonic acid in water (25 °C).   Therefore, an ideal reaction of the present mineralization is written, as follows:

$$Ca^{2+} + HCO_3^- \rightarrow CaCO_3 \downarrow + H^+ \tag{1}$$
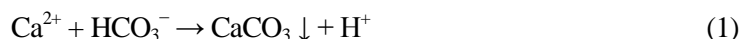
If the matrix polymer has a functional group such as -COO$^-$ to capture Ca^{2+} [35], there will occur an efficient progress of the CaCO$_3$ formation inside the matrix, with regular refreshment of the outer ion server.   The reaction of Eq. (1) accompanying deprotonation of HCO$_3^-$ is also concerned in the actual biomineralization made in shellfish, coral, etc. under the sea [31,39].

In the following two subsections, the successful CaCO$_3$ deposition inward the chiral nematic CNC/polymer films is demonstrated by EDX and WAXD study.   The retention of chiral nematic organization in the final products is proved in *Sect. 3.3.1* (see, for instance, FE-SEM data in Fig. 5).   Since those mineralized films (dried) were covered with white precipitation to a certain extent, they were subjected to the measurements after the surfaces were rubbed with sandpaper.   The polished films were slightly translucent, but transmitted light.

3.2.2. Internal exploration by EDX analysis

EDX measurements were made using fracture surfaces of mineralized CNC/polymer films.   Fig. 2 illustrates the mapping of Ca element for the fractured films of *m*-9CNC/P(HEMA$_{90}$-*co*-AA$_{10}$)_1d (part a) and *m*-9CNC/P(HEMA$_{90}$-*co*-AA$_{10}$)_5d (part b); these mineralized samples were obtained via 1-day-soaking and 5-day-soaking treatments, respectively, of 9CNC/P(HEMA$_{90}$-*co*-AA$_{10}$).   A low-magnification micrograph given in Fig. 2c is a SEM image of the corresponding area, taken for *m*-9CNC/P(HEMA$_{90}$-*co*-AA$_{10}$)_1d.   As can be seen from the mapping data, Ca elements were widely distributed inside the film mineralized for 1 day, and the density was further elevated by the 5-day treatment.   Such uniform distribution of Ca throughout the matrix inside was confirmed for all the explored samples mineralized over the period of 1–5 days.
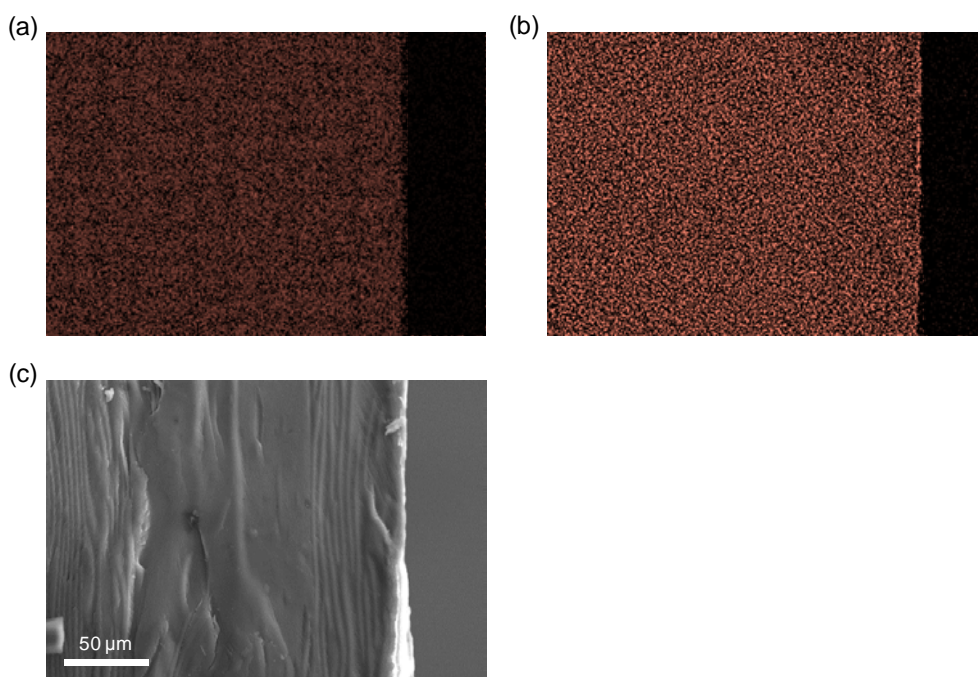
10

Fig. 2. EDX mapping of element Ca for the fracture surfaces of (a) m-9CNC/P(HEMA$_{90}$-co-AA$_{10}$)_1d and (b) m-9CNC/P(HEMA$_{90}$-co-AA$_{10}$)_5d. Part (c) illustrates a SEM image of the corresponding area, taken for the fractured film of (a).

The cross-sectional analysis by EDX also offered numeric data (atom (At) %) about the allocation of four elements C, O, S, and Ca in the mineralized CNC/polymer films (see Supplementary Materials, Table S1). For example, using the samples shown in Fig. 2, we obtained the following At % data: 73.1 C, 26.4 O, 0.07 S, and 0.49 Ca for m-9CNC/P(HEMA$_{90}$-co-AA$_{10}$)_1d; 71.4 C, 27.6 O, 0.07 S, and 0.91 Ca for m-9CNC/P(HEMA$_{90}$-co-AA$_{10}$)_5d. Assuming that all the calcium formed CaCO$_3$ (formula weight, 100), ideally the mineral would occupy 3.71 wt% in the former hybrid material and 6.81 wt% in the latter one. In Fig. 3, the relative amount of Ca incorporated into the mineralized films of 9CNC/PHEMA and 9CNC/P(HEMA$_y$-co-AA$_{(100-y)}$) are plotted as a function of the AA proportion $(100-y)$ in the vinyl polymer. The plots also make a comparison between two terms, 1 day ($n = 1$) and 5 days ($n = 5$), of the mineralization treatment. The Ca allocation in the films of m-9CNC/PHEMA_nd ($n = 1, 5$) was generally low (Ca $\leq$ 0.1 At %). In the case where the copolymer P(HEMA-co-AA) was employed for the matrix polymer, a relatively larger amount of Ca

11

was introduced into the mineralized films. The Ca % was always higher in the samples mineralized for the longer period ($n = 5$), and, decidedly, the value increased with increasing AA proportion in the copolymer composition. This indicates that the AA constituent largely contributed to the capture of Ca^{2+} in the composite films.
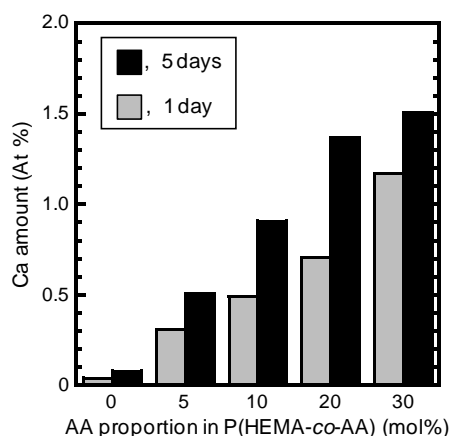

Fig. 3. Ca amount (in At %) incorporated in the films of m-9CNC/PHEMA_nd and m-9CNC/P(HEMA_y-co-AA_$(100-y)$)_nd ($n = 1, 5$), plotted as a function of the AA proportion ($100-y$) in the vinyl polymer.

In a similar EDX analysis for mineralized P(HEMA_90-co-AA_10) films free of CNC, the following Ca allocation data were obtained: 0.39 At % for m-P(HEMA_90-co-AA_10)_1d and 0.78 At % for P(HEMA_90-co-AA_10)_5d. In comparison with these data, the Ca gains of m-9CNC/P(HEMA_90-co-AA_10)_1d (Ca, 0.49 At %) and m-9CNC/P(HEMA_90-co-AA_10)_5d (Ca, 0.91 At %) are evidently higher, suggesting that the surface-SO_3^- groups of CNC would also contribute to the taking-in of Ca^{2+} by the composite films. However, the apparent Ca % declined when the CNC concentration increased to $x = 11$, as exemplified by the data of 0.33 At % and 0.56 At % for m-11CNC/P(HEMA_90-co-AA_10)_1d and _5d films, respectively (see Table S1). This observation is caused by the substantial decrease of the AA content in the matrix whole and also by the lowering in the degree of swelling of the matrix.

3.2.3. Evaluation of CaCO$_3$ polymorphs by WAXD

12

Fig. 4 illustrates WAXD intensity curves obtained for mineralized films of 9CNC/PHEMA and 9CNC/P(HEMA$_{80}$-co-AA$_{20}$) series.   The data (**i**–**iv**) in Fig. 4a serve to see a typical transformation of WAXD profile accompanying the mineralization treatment of CNC/PHEMA composites.   Before mineralization, as shown by data a-**i**, the sample 9CNC/PHEMA gave several diffraction peaks coming from the monoclinic Iβ [40] of cellulose (CNC here), except a diffuse scattering halo centered at $2\theta = 18.5°$ derived from the vinyl polymer.   This WAXD pattern was apparently unchanged in m-9CNC/PHEMA_1d obtained via 1-day soaking for mineralization.   After treatment for 3 days, the product m-9CNC/PHEMA_3d exhibited a diffraction profile evidencing the deposition of crystalline CaCO$_3$ in the inside of film, as shown by data a-**ii**.   This crystal was identified as vaterite, a metastable crystal of CaCO$_3$; the peak assignments in the WAXD data are made using the following hexagonal lattice parameters, $a = b = 4.13$ Å, $c = 8.49$ Å, and $\gamma = 120°$ [41].   Further treatment over a 5-day period resulted in occurrence of a more stable CaCO$_3$ crystal, aragonite, besides vaterite, in the product m-9CNC/PHEMA_5d, as shown by data a-**iii**, where the diffraction peaks from aragonite are indexed in terms of its standard orthorhombic crystal form ($a = 4.961$ Å, $b = 7.967$ Å, and $c = 5.740$ Å) [42].   In contrast, a reference sample m-PHEMA_5d deposited only a trace amount of vaterite inside the film (data a-**iv**).   In a supplementary examination by FT-IR for 1-day-treated samples, m-PHEMA_1d and m-9CNC/PHEMA_1d, there was no CaCO$_3$ in the former, while the so-called ACC (i.e., amorphous calcium carbonate) was deposited in the latter (see spectral data in Fig. S2a and b).

In Table 1 (upper two rows), the CaCO$_3$ polymorphs observed for the mineralization of the CNC/PHEMA series are summarized, in comparison with the case using PHEMA alone.   The result suggests that the surface-sulfated CNC contributed to the easier start and subsequent moderate progress of the calcic mineralization. Regarding the time-course of the polymorphic change, we can suppose a transition scheme from ACC as precursor to the stable aragonite crystal through vaterite as intermediate.   As a rare case, we perceived another stable crystal, calcite, besides vaterite and aragonite, slightly appearing in a mineralized film of $x = 11$, m-11CNC/PHEMA_5d (see Fig. S3a).
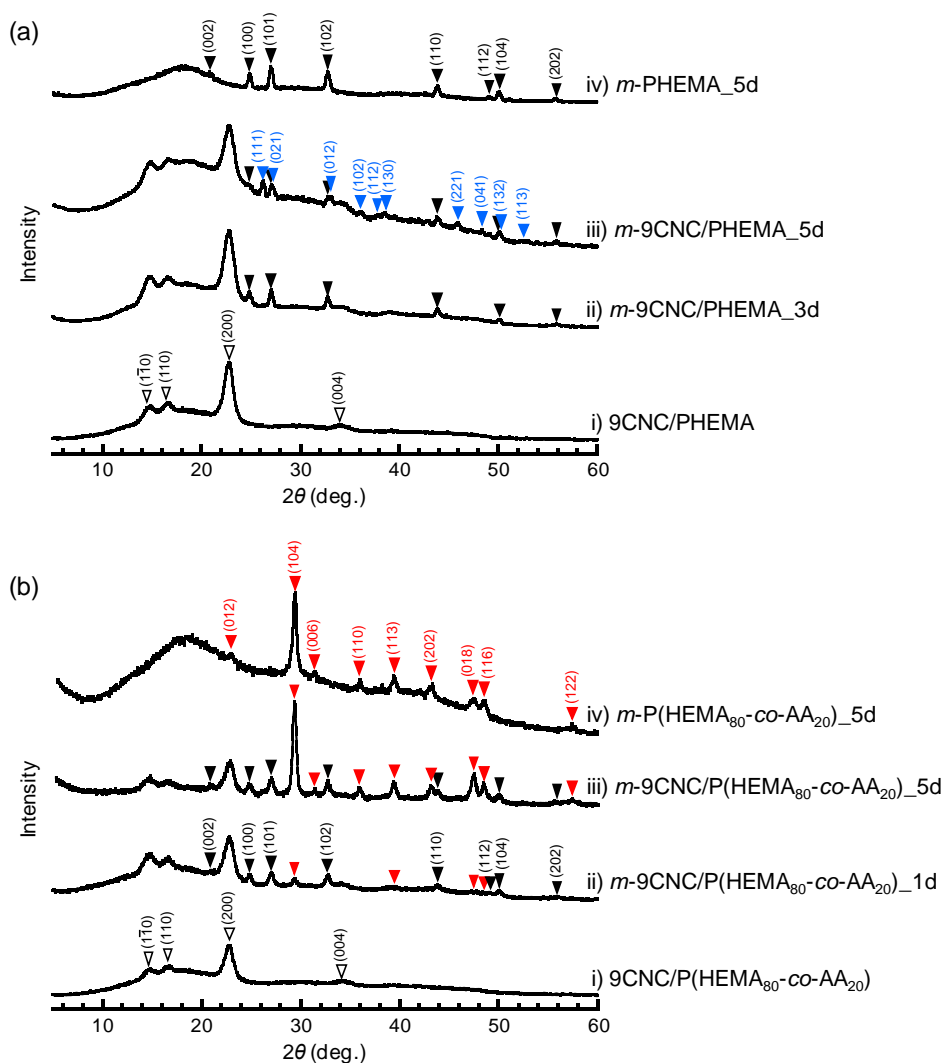
13

Fig. 4. WAXD intensity profiles for mineralized films of (a) 9CNC/PHEMA series and (b) 9CNC/P(HEMA$_{80}$-co-AA$_{20}$) series. Black, blue, and red arrows indicate a diffraction coming from vaterite, aragonite, and calcite crystals, respectively. In data of nonmineralized CNC/polymer films (data a-**i** and b-**i**), major diffraction peaks from cellulose Iβ are marked by white arrows.

Table 1. CaCO$_3$ polymorphs observed for various film samples mineralized for 1–5 days

Matrix	Soaking treatment period		
	1 day	3 days	5 days
m-PHEMA	no deposition	Vat	Vat
m-CNC/PHEMA[a]	ACC	Vat	Ara + Vat
m-P(HEMA-co-AA)	no deposition[†]	Cal	Cal
m-CNC/P(HEMA-co-AA)[b]	Cal + Vat	Cal + Vat	Cal + Vat[‡]

Notations: ACC, amorphous calcium carbonate; Vat, vaterite; Ara, aragonite; Cal, calcite.

[a] xCNC/PHEMA films of x = 7 and 9 were mainly used for the matrix.

14

[b] 9CNC/P(HEMA$_y$-co-AA$_{(100-y)}$) of HEMA:AA = 95:5–70:30 were used for the matrix.

[†] Mineral formation was not clearly observed, but calcium was noted in the ionic form combined with the AA unit of P(HEMA-co-AA).

[‡] As regards the data obtained after 5-day mineralization, a relatively AA-poor sample m-9CNC/P(HEMA$_{95}$-co-AA$_5$)_5d imparted precipitation of aragonite, besides calcite and vaterite, and, contrastively, only calcite deposition prevailed in m-9CNC/P(HEMA$_{70}$-co-AA$_{30}$)_5d richer in the AA amount.

Concerning the CNC/P(HEMA-co-AA) copolymer series, a different transition of CaCO$_3$ polymorph was observed in the mineralization process. The four data (**i**–**iv**) in Fig. 4b serve to specify a typical transformation of WAXD profile accompanying the mineralization of 9CNC/P(HEMA$_{80}$-co-AA$_{20}$) that is a representative sample of the series. In data b-**i** for the nonmineralized film, we solely find the diffraction peaks from CNCs of Iβ and an amorphous halo (2$\theta \approx$ 18°) from the vinyl copolymer. After 1-day mineralization, the product m-9CNC/P(HEMA$_{80}$-co-AA$_{20}$)_1d already deposited crystalline CaCO$_3$ in the inside, differing from the situation (ACC only) in m-9CNC/PHEMA_1d. As indicated in data b-**ii**, the formed crystals were actually a mixture of two polymorphs, vaterite and calcite, the latter being the most stable CaCO$_3$ crystal with a trigonal form ($a = b =$ 4.98 Å, c = 17.06 Å, and γ = 120°) [43]. As the mineralization period lengthened into 3–5 days, the diffraction peaks from calcite became more prominent rather than those from vaterite. This is demonstrated by data b-**iii** for m-9CNC/P(HEMA$_{80}$-co-AA$_{20}$)_5d; the calcite prevalence was surely more impressive for the WAXD intensity. In a control experiment using P(HEMA$_{80}$-co-AA$_{20}$) per se, there appeared only calcite deposition in the 3-day- and 5-day-mineralized products, as instantiated by data b-**iv** for m-P(HEMA$_{80}$-co-AA$_{20}$)_5d.

The transition scheme of CaCO$_3$ polymorph observed for the CNC/P(HEMA-co-AA) series and that for the reference copolymer are summarized in the lower two rows of Table 1. Plainly, the AA constituent of the matrices can be taken as contributing to the prevalence of the calcite formation. In further support of this, we confirmed that only calcite deposition prevailed in a relatively AA-richer sample, m-9CNC/P(HEMA$_{70}$-co-AA$_{30}$)_5d, whereas another product m-9CNC/P(HEMA$_{95}$-co-AA$_5$)_5d imparted a formation of aragonite, besides calcite and vaterite (see WAXD data in Fig. S3b and c). The latter result of aragonite detection is ascribable to the large occupation of the matrix by the CNC and HEMA ingredients, which should be rationalized by the similar observation (e.g., data a-**iii** in Fig. 4) for the CNC/PHEMA series.

In the mineralization of the CNC/P(HEMA-*co*-AA) series, there are basically two independent pathways leading to the deposition of crystalline $CaCO_3$ (ideally calcite). The two, termed P-I and P-II, are different from each other in the starting site and kinetics of structure development. In P-I, Ca^{2+} cations are preferentially captured in a complex form such as $2C_2H_3\text{-}COO^-\text{----}Ca^{2+}$ by the AA absorbent of the matrix copolymer (see a supporting IR data in Fig. S2c), and they can readily combine with diffusing HCO_3^- to yield $CaCO_3$ (Eq. (1)). The smoothly initiated and repeated reactions would make a direct process up to the most stable calcite phase, without producing less-ordered or metastable intermediate phases in the practical time scale. This rapid kinetics explains the polymorphic observations for the mineralized samples of 9CNC/P(HEMA-*co*-AA) with HEMA/AA = 90:10–70:30. In P-II, HCO_3^- anions can combine with Ca^{2+} that is trapped in the vicinity of CNC surfaces by interaction such as $2CNC\text{-}OSO_3^-\text{----}Ca^{2+}$. However, the frequency of the successful combination in the swollen matrix would be rather low, because the concentration of the sulfated functional groups is absolutely low and the Ca^{2+} retention by the acidic CNC adsorbent may be potentially tenacious. Therefore, the mineralization following P-II is controlled by a relatively slower kinetics. This slow process permits the appearance of various intermediate phases (ACC, vaterite, and aragonite) in the samples of CNC/PHEMA and CNC/P(HEMA-*co*-AA) short of AA, each mineralized in different terms of 1–5 days.

3.3. Mineralization effects on mesomorphic structure and thermal property

3.3.1. Evaluation of chiral nematic pitch by FE-SEM

Fig. 5 displays FE-SEM images of two fractured films, making a comparison of the internal morphology between a nonmineralized sample 11CNC/P(HEMA$_{90}$-*co*-AA$_{10}$) and the mineralized product *m*-11CNC/P(HEMA$_{90}$-*co*-AA$_{10}$)_5d. We can see a well-developed periodic architecture corresponding to the fingerprint texture in the interior of both film specimens. As illustrated by the result, all the mineralized composite films explored in this study retained the chiral nematic organization as they did before soaking treatment for the mineralization. However, the pitch *P* became considerably decreased after the treatment; for example, we estimated *P* = 2.52 μm (on average) for *m*-11CNC/P(HEMA$_{90}$-*co*-AA$_{10}$)_5d from the SEM image, the value

seriously falling from $P = 4.91$ μm observed before mineralization.   Table 2 summarizes P data thus obtained by

FE-SEM for $CaCO_3$-deposited films with various compositions of CNC/PHEMA and CNC/P(HEMA-*co*-AA),

together with the data for the starting nonmineralized samples.   We can find a definite trend of P decreasing with

an increase in the treatment time; strictly, the diminution of P value is particularly large in the first term of 24 h.

In the course of the mineralization treatment, the CNC/polymer matrices were swollen with the aqueous solution

containing essential ions such as Ca^{2+} and evolved H^+.   As we referred to the matter in *Sect. 3.1* for the CNC

lyotropics in HEMA/AA/water, the electrolytic effect [6] shortening P (i.e., strengthening helical twist) may also

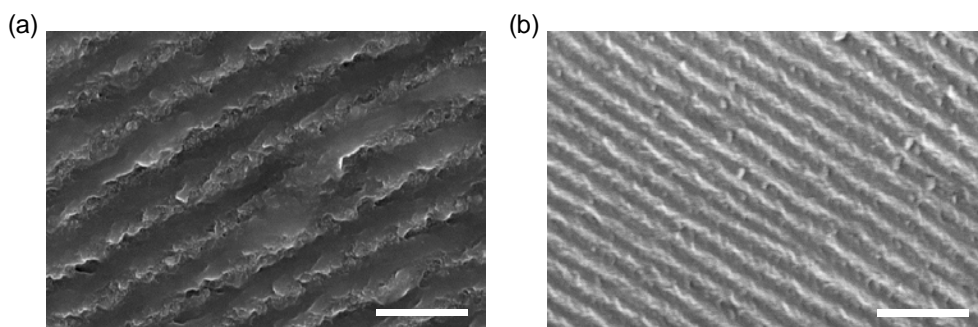be applicable to the chiral nematic system of CNC/polymer hydrogel.

Fig. 5.   FE-SEM images of fracture surface morphology for film specimens of (a) 11CNC/P(HEMA$_{90}$-*co*-AA$_{10}$)

(not mineralized) and (b) *m*-11CNC/P(HEMA$_{90}$-*co*-AA$_{10}$)_5d (mineralized for 5 days).   Scale bar denotes 5 μm.

Table 2.   Values of chiral nematic pitch (P) for various composites of CNC/PHEMA and

CNC/P(HEMA-*co*-AA) series, estimated by FE-SEM measurements before treatment and after 1-day and 5-day

treatments for $CaCO_3$ mineralization

Sample	P (μm)		
	Before	1 day	5 day
7CNC/PHEMA	9.85	7.94	7.07
9CNC/PHEMA	9.11	6.53	6.39
11CNC/PHEMA	7.28	6.00	5.55
7CNC/P(HEMA$_{90}$-*co*-AA$_{10}$)	7.61	n.d.	4.95
9CNC/P(HEMA$_{90}$-*co*-AA$_{10}$)	7.43	5.16	4.68
11CNC/P(HEMA$_{90}$-*co*-AA$_{10}$)	4.91	n.d.	2.52
9CNC/P(HEMA$_{95}$-*co*-AA$_5$)	8.28	5.44	4.80

17

9CNC/P(HEMA$_{80}$-*co*-AA$_{20}$)	6.82	4.91	4.57
9CNC/P(HEMA$_{70}$-*co*-AA$_{30}$)	4.27	3.93	3.60

n.d.; not measured.

With regard to the dimensions of the CaCO$_3$ incorporated in the mineralized films, the deposits were not perceptible even at magnifications of the SEM data, probably being distributed as nano-sized precipitates between the chiral nematic stratums.   Actually, from the half-height width of major WAXD peaks (such as (104) of calcite and (101) of vaterite) detected for the mineralized samples, the crystalline sizes were estimated to be ca. 15–25 nm by using a conventional Scherrer's method [44].   The sizes are smaller than the interlayer spacing of 25–40 nm [45] evaluated formerly for the chiral nematic layered structures developing in aqueous CNC suspensions.   It may be possible that even such a minute mineral deposition expands the distance between adjacent nematic layers to some extent.   Nevertheless, the helical pitch *P* diminished following the mineralization, as stated above. Presumably, the effect of ionic additives arising prior to the mineral deposition was more intense and readily invited a marked increase in the angular difference between the adjacent nematic directors.   This change in the twist angle of the chiral nematic arrangement is responsible for the lowering in *P* value.

3.3.2. Thermal resistant property evaluated by TGA

Fig. 6 displays TGA curves obtained for two mineralized composites, *m*-9CNC/PHEMA_5d (part a) and *m*-9CNC/P(HEMA$_{90}$-*co*-AA$_{10}$)_5d (part b), each data being compared with that of the corresponding nonmineralized composite.   In the TGA curves of the nonmineralized samples, a primary degradation stage characteristic of CNCs' pyrolysis can be observed, in common, in the range of ca. 180–300 °C, which must be a drawback in the thermal stability of polymer materials with CNC fillers.   As suggested by earlier reports [23,46], this degradation of CNCs would be accompanied by a dehydration reaction involving the hydroxyl groups and, deservedly, catalyzed by the sulfo groups lying on the CNC surfaces.   In the subsequent stage above 300 °C, besides a relatively slow decomposition of CNCs, the vinyl polymers rapidly lose the entire weight in the range of 300–450 °C (for PHEMA) or 350–470 °C (for P(HEMA$_{90}$-*co*-AA$_{10}$)).   The slow and fast decompositions of the

18

CNC and vinyl polymers, respectively, were confirmed in a control experiment.　Eventually the nonmineralized composites yielded a char as residue of <5% at 600–700 °C, which is mainly derived from the CNC component.
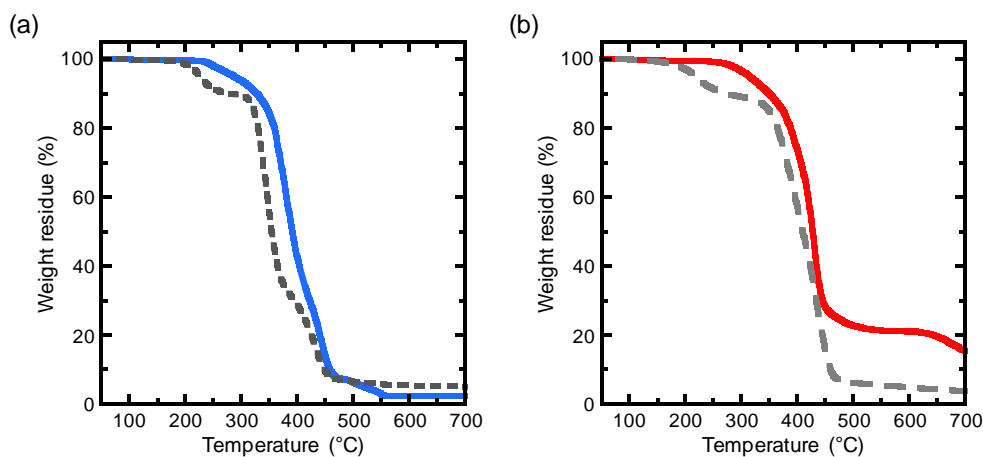

Fig. 6.　TGA data obtained for various film specimens: (a) 9CNC/PHEMA (dotted line in black) and *m*-9CNC/PHEMA_5d (solid line in blue); (b) 9CNC/P(HEMA$_{90}$-*co*-AA$_{10}$) (dashed line in gray) and *m*-9CNC/P(HEMA$_{90}$-*co*-AA$_{10}$)_5d (solid line in red).

After mineralization of the pristine composite films, the primary degradation stage of CNCs disappeared and the onset temperature of decomposition (T_d) of the respective samples moved upward explicitly.　More quantitatively, we observed a T_d elevation of 50 °C for *m*-9CNC/PHEMA_5d (see Fig. 6a) and that of 103 °C for *m*-9CNC/P(HEMA$_{90}$-*co*-AA$_{10}$)_5d (see Fig. 6b) relative to the situation before mineralization.　Such an improvement in heat resistance of the composites is interpreted as being due to suppression of the sulfo-catalytic dehydration of CNCs.　The inactivation of the CNC's self-catalysis supports the calcium adsorption onto the sulfated CNCs, followed by CaCO$_3$ deposition nearby the CNC surfaces (but this inorganic allocation is generally small), which was an expected route of mineralization in the present wet process.

In the meantime, we can find a large difference in the weight retention behavior above 500 °C between the two mineralized series of CNC/polymer composites.　In this kind of TGA test, the so-called flame resistance of polymeric materials is evaluated usually from the weight residue at such high temperatures.　As seen in Fig. 6a, the weight residue at 550–700 °C of *m*-9CNC/PHEMA_5d and that of the original 9CNC/PHEMA sample are at

almost the same level of 3–5%. As shown by the EDX study (*Sect. 3.2.1*), the inorganic content in *m*-9CNC/PHEMA_5d was quite low; i.e., Ca ≈ 0.1 At % and $CaCO_3$ < 0.7 wt%. Plainly, this shortage of mineral deposit is responsible for the observation of no improvement in flame resistance for the CNC/PHEMA series. In contrast, the weight residue at 500–700 °C of *m*-9CNC/P(HEMA$_{90}$-*co*-AA$_{10}$)_5d was much higher than that of the nonmineralized composite (see Fig. 6b); specifically, the difference in the residue was 17% at 500–635 °C and 16–12% at 640–700 °C. It is thus clear for this CNC/P(HEMA-*co*-AA) series that the mineralization led to a marked improvement in flame resistance of the polymer composite film. In the EDX analysis, the inorganic content in *m*-9CNC/P(HEMA$_{90}$-*co*-AA$_{10}$)_5d was assessed as follows; Ca = 0.91 At % and $CaCO_3$ = 6.81 wt% (at the maximum). Here we notice that the increment in weight residue, 17–12%, observed at 500–700 °C exceeds the $CaCO_3$ amount, 6.81 wt%; this indicates a synergistic effect of the carbonate nano-hybridization on the resistance to pyrolysis of the CNC/polymer matrix. Incidentally, the slight weight-loss observed above 640 °C for the mineralized sample may be ascribed to the dissociation of $CaCO_3$ into CaO (+ CO_2) [47], and this dissociation would be involved chiefly with the metastable vaterite mingled with the major polymorph, calcite, of the deposited minerals (see *Sect. 3.2.3*).

4. Conclusions

Partly biomimetic $CaCO_3$ mineralization was carried out using CNC/PHEMA and CNC/P(HEMA-*co*-AA) films wherein a chiral nematic CNC assembly was immobilized in advanced by polymerization of the aqueous monomer solvent (HEMA/AA) for suspending CNCs. The mineralization was successfully done in a batchwise operation by immersing and swelling the CNC/polymer films in a low-basic salt solution (pH ≤ 9) providing Ca^{2+} and HCO_3^- ions. A relatively small amount of $CaCO_3$ was deposited inside the CNC/PHEMA films, in the form of metastable crystal (vaterite/aragonite) or non-crystalline ACC. The CNC/P(HEMA-*co*-AA) films, preferably, incorporated the most stable $CaCO_3$ crystal, calcite, in a deposit amount commensurate to the AA content. The mesogenic CNC and the AA unit in the sustaining polymer, both bearing an anionic group (-SO_3^- or -COO^-), contributed to capturing Ca^{2+} to facilitate the $CaCO_3$ deposition in the swollen film matrix; however, the crystal

development onto the CNC scaffold obeyed a rather slower kinetics compared with the crystallization from AA-carboxyl sites.

The mineralized films, *m*-CNC/PHEMA and *m*-CNC/P(HEMA-*co*-AA), retained the chiral nematic arrangement, but the helical pitch was appreciably reduced relative to that observed before the mineralization. This reduction was invited by an effect of various ionic entities required for the mineralization process, the electrolytes strengthening the helical twist of the CNC chiral nematics. It was also found that the inorganic hybridization improved the heat resistance of the CNC/polymer films, elevating the T_d by as much as 50–100 °C. In particular, the weight residue to pyrolysis (therefore flame resistance) of the CNC/P(HEMA-*co*-AA) series was markedly enhanced by the $CaCO_3$ (calcite) deposition.

In the present study, the helical pitch of the chiral nematic structure preserved in the mineralized CNC/polymer composites was in the range of a few to 10 micrometers. If the effect of electrolytic additives is used more positively in artifice, the pitch would be further shortened to a scale of several hundreds of nanometers; then the resulting hybrid materials should be iridescent. The preparation and characterization of such mineralized and colored composites are topics that remain to be described in the near future.

Declaration of competing interest

The authors declare no conflict of interest.

Acknowledgments

Appendix A. Supplementary data

Supplementary data related to this article can be found online at http://doi.org/10.1016/j.ijbiomac.??????.

21

References

[1] J.-F. Revol, H. Bradford, J. Giasson, R.H. Marchessault, D.G. Gray, Helicoidal self-ordering of cellulose microfibrils in aqueous suspension, Int. J. Biol. Macromol. 14 (1992) 170–172.

[2] Y. Habibi, L.A. Lucia, O.J. Rojas, Cellulose nanocrystals: chemistry, self-assembly, and applications, Chem. Rev. 110 (2010) 3479–3500.

[3] D. Klemm, F. Kramer, S. Moritz, T. Lindström, M. Ankerfors, D.G. Gray, A. Dorris, Nanocelluloses: a new family of nature-based materials, Angew. Chem. Int. Ed. 50 (2011) 5438–5466.

[4] R.J. Moon, A. Martini, J. Nairn, J. Simonsen, J. Youngblood, Cellulose nanomaterials review: structure, properties and nanocomposites, Chem. Soc. Rev. 40 (2011) 3941–3994.

[5] T. Abitbol, A. Rivkin, Y. Cao, Y. Nevo, E. Abraham, T. Ben-Shalom, S. Lapidot, O. Shoseyov, Nanocellulose, a tiny fiber with huge applications, Curr. Opin. Biotechnol. 39 (2016) 76–88.

[6] X.M. Dong, T. Kimura, J.-F. Revol, D.G. Gray, Effects of ionic strength on the isotropic–chiral nematic phase transition of suspensions of cellulose crystallites, Langmuir 12 (1996) 2076–2082.

[7] X.M. Dong, J.-F. Revol, D.G. Gray, Effect of microcrystallite preparation conditions on the formation of colloid crystals of cellulose, Cellulose 5 (1998) 19–32.

[8] D.G. Gray, Chiral nematic ordering of polysaccharides, Carbohydr. Polym. 25 (1994) 277–284.

[9] J.-X. Guo, D.G. Gray, Lyotropic cellulosic liquid crystals, in: R.D. Gilbert (Ed.), Cellulosic polymers, blends and composites, Hanser, Munich, 1994, Chapter 2.

[10] P. Zugenmaier, Polymer solvent interaction in lyotropic liquid crystalline cellulose derivative systems, in: R.D. Gilbert (Ed.), Cellulosic polymers, blends and composites, Hanser, Munich, 1994, Chapter 4.

[11] P. Zugenmaier, Supramolecular structure of polysaccharides, in: S. Dumitriu (Ed.), Polysaccharides: structural diversity and functional versatility, Marcel Dekker, New York, 1998, Chapter 2.

[12] Y. Nishio, J. Sato, K. Sugimura, Liquid crystals of cellulosics: fascinating ordered structures for the design of functional material systems, Adv. Polym. Sci. 271 (2016) 241–286.

[13] Y. Nishio, Material functionalization of cellulose and related polysaccharides via diverse microcompositions, Adv. Polym. Sci. 205 (2006) 97–151.

[14] Y. Nishio, T. Yamane, T. Takahashi, Morphological studies of liquid-crystalline cellulose derivatives. I. Liquid-crystalline characteristics of hydroxypropyl cellulose in 2-hydroxyethyl methacrylate solutions and in polymer composites prepared by bulk polymerization, J. Polym. Sci., Polym. Phys. Ed. 23 (1985) 1043–1052.

[15] Y. Nishio, S. Susuki, T. Takahashi, Structural investigations of liquid-crystalline ethylcellulose, Polym. J. 17 (1985) 753–760.

[16] R. Chiba, Y. Nishio, Y. Sato, M. Ohtaki, Y. Miyashita, Preparation of cholesteric (hydroxypropyl)cellulose/polymer networks and ion-mediated control of their optical properties, Biomacromolecules 7 (2006) 3076–3082.

[17] E. Dujardin, M. Blaseby, S. Mann, Synthesis of mesoporous silica by sol–gel mineralisation of cellulose nanorod nematic suspensions, J. Mater. Chem. 13 (2003) 696–699.

[18] A. Thomas, M. Antonietti, Silica nanocasting of simple cellulose derivatives: towards chiral pore systems with long-range order and chiral optical coatings, Adv. Funct. Mater. 13 (2003) 763–766.

[19] K.E. Shopsowitz, H. Qi, W.Y. Hamad, M.J. MacLachlan, Free-standing mesoporous silica films with tunable chiral nematic structures, Nature 468 (2010) 422–425.

[20] J. Sato, K. Sugimura, Y. Teramoto, Y. Nishio, Preparation and chiroptical properties of cellulose chlorophenylcarbamate–silica hybrids having a chiral nematic mesomorphic structure, Polymer 173 (2019) 172–181.

[21] M. Giese, L.K. Blusch, M.K. Khan, M.J. MacLachlan, Functional materials from cellulose-derived liquid-crystal templates, Angew. Chem. Int. Ed. 54 (2015) 2888–2910.

[22] W.Y. Hamad, Photonic and semiconductor materials based on cellulose nanocrystals, Adv. Polym. Sci. 271 (2016) 287–328.

[23] M. Tatsumi, Y. Teramoto, Y. Nishio, Polymer composites reinforced by locking-in a liquid-crystalline assembly of cellulose nanocrystallites, Biomacromolecules 13 (2012) 1584–1591.

[24] M. Tatsumi, F. Kimura, T. Kimura, Y. Teramoto, Y. Nishio, Anisotropic polymer composites synthesized by immobilizing cellulose nanocrystal suspensions specifically oriented under magnetic fields, Biomacromolecules 15 (2014) 4579–4589.

[25] T. Ogiwara, A. Katsumura, K. Sugimura, Y. Teramoto, Y. Nishio, Calcium phosphate mineralization in cellulose derivative/poly(acrylic acid) composites having a chiral nematic mesomorphic structure, Biomacromolecules 16 (2015) 3959–3969.

[26] S. Mann, Biomineralization: principles and concepts in bioinorganic materials chemistry, Oxford University Press, Oxford, 2001.

[27] N.A.J.M. Sommerdijk, G. de With, Biomimetic $CaCO_3$ mineralization using designer molecules and interfaces, Chem. Rev. 108 (2008) 4499–4550.

[28] L.B. Gower, Biomimetic model systems for investigating the amorphous precursor pathway and its role in biomineralization, Chem. Rev. 108 (2008) 4551–4627.

[29] A. Arakaki, K. Shimizu, M. Oda, T. Sakamoto, T. Nishimura, T. Kato, Biomineralization-inspired synthesis of functional organic/inorganic hybrid materials: organic molecular control of self-organization of hybrids, Org. Biomol. Chem. 13 (2015) 974–989.

[30] B. Cantaert, D. Kuo, S. Matsumura, T. Nishimura, T. Sakamoto, T. Kato, Use of amorphous calcium carbonate for the design of new materials, ChemPlusChem 82 (2017) 107–120.

[31] M. Cusack, A. Freer, Biomineralization: elemental and organic influence in carbonate systems, Chem. Rev. 108 (2008) 4433–4454.

[32] J.L. Arias, M.S. Fernández, Polysaccharides and proteoglycans in calcium carbonate-based biomineralization, Chem. Rev. 108 (2008) 4475–4482.

[33] A. George, A. Veis, Phosphorylated proteins and control over apatite nucleation, crystal growth, and inhibition, Chem. Rev. 108 (2008) 4670–4693.

[34] L.C. Palmer, C.J. Newcomb, S.R. Kaltz, E.D. Spoerke, S.I. Stupp, Biomimetic systems for hydroxyapatite mineralization inspired by bone and enamel, Chem. Rev. 108 (2008) 4754–4783.

[35] A. Katsumura, K. Sugimura, Y. Nishio, Calcium carbonate mineralization in chiral mesomorphic order-retaining ethyl cellulose/poly(acrylic acid) composite films, Polymer 139 (2018) 26–35.

[36] J.-F. Revol, L. Godbout, D.G. Gray, Solid self-assembled films of cellulose with chiral nematic order and optically variable properties, J. Pulp Paper Sci. 24 (1998) 146–149.

[37] T. Iwatsubo, T. Yamaguchi, Hypercomplex gel changes to organic/inorganic solid solution by phase transition in an artificial biomineralization system, Polym. J. 40 (2008) 958–964.

[38] R.C. Weast, M.J. Astle (Eds.), Handbook of Chemistry and Physics, 61st ed, CRC Press, Florida, 1981, pp. D-165–167.

[39] M. Inoue, N. Gussone, Y. Koga, A. Iwase, A. Suzuki, K. Sakai, H. Kawahata, Controlling factors of Ca isotope fractionation in scleractinian corals evaluated by temperature, pH and light controlled culture experiments, Geochim. Cosmochim. Acta 167 (2015) 80–92.

[40] J. Sugiyama, R. Vuong, H. Chanzy, Electron diffraction study on the two crystalline phases occurring in native cellulose from an algal cell wall, Macromolecules 24 (1991) 4168–4175.

[41] Powder Diffraction File (PDF) No. 00-000-2788, International Centre for Diffraction Data.

[42] Powder Diffraction File (PDF) No. 01-071-2392, International Centre for Diffraction Data.

[43] Powder Diffraction File (PDF) No. 01-086-2334, International Centre for Diffraction Data.

[44] L.E. Alexander, X-Ray diffraction methods in polymer science, Wiley-Interscience, New York, 1969, Chapter 7.

[45] C. Schütz, M. Agthe, A.B. Fall, K. Gordeyeva, V. Guccini, M. Salajková, T.S. Plivelic, J.P.F. Lagerwall, G. Salazar-Alvarez, L. Bergström, Rod packing in chiral nematic cellulose nanocrystal dispersions studied by small-angle X-ray scattering and laser diffraction, Langmuir 31 (2015) 6507–6513.

[46] M. Roman, W.T. Winter, Effect of sulfate groups from sulfuric acid hydrolysis on the thermal degradation behavior of bacterial cellulose, Biomacromolecules 5 (2004) 1671–1677.

[47] I. Halikia, L. Zoumpoulakis, E. Christodoulou, D. Prattis, Kinetic study of the thermal decomposition of calcium carbonate by isothermal methods of analysis, Eur. J. Miner. Process. Environ. Prot. 1 (2001) 89–102.

ABSTRACT: $CaCO_3$ mineralization was carried out using cellulose nanocrystal (CNC)/polymer composites wherein a chiral nematic structure of CNC assembly was immobilized in advance via a polymerization process of the precursory aqueous CNC/vinyl monomer lyotropics (7–11 wt% CNC in feed). Two series of polymer composites were prepared: CNC/poly(2-hydroxyethyl methacrylate) (PHEMA) and CNC/poly(2-hydroxyethyl methacrylate-*co*-acrylic acid) (P(HEMA-*co*-AA), HEMA:AA = 95:5–70:30 in mol). The mineralization was allowed to proceed solely by soaking the composite films in a salt solution containing Ca^{2+} and HCO_3^- under a low-basic condition (pH $\leq$ 9). Polymorphism of $CaCO_3$ deposited inside the films was examined by X-ray diffractometry as a function of the soaking time (1–5 day) and also of the matrix composition. In the CNC/PHEMA series, the polymorphic form changed from amorphous calcium carbonate (ACC) (1-day soaking) to metastable crystalline vaterite (3-day soaking) and then to a mixture of vaterite and aragonite (5-day soaking). In the mineralization of the CNC/P(HEMA-*co*-AA) series, the formation of stable calcite was prominent besides minor appearance of vaterite. It was deduced that the mesofiller CNC and the AA unit in the vinyl polymer, both bearing an anionic group ($-SO_3^-$ or $-COO^-$), contributed to capturing Ca^{2+} to facilitate the $CaCO_3$ deposition in the swollen film matrix. The pre-invested chiral nematic organization was kept in any of the mineralized films (dried); however, the helical pitch was appreciably reduced relative to that observed before the mineralization, attributable to the increase of ionic strength in the CNCs' surroundings accompanied by the wet process. Thermogravimetry showed that the mineralization definitely improved the thermal performance (heat/flame resistance) of the mesomorphic order-retaining CNC/polymer composites.

Graphical Abstracts

CaCO₃ mineralization in polymer composites with cellulose nanocrystals providing a chiral nematic mesomorphic structure

Yukiko Nakao, Kazuki Sugimura*, and Yoshiyuki Nishio
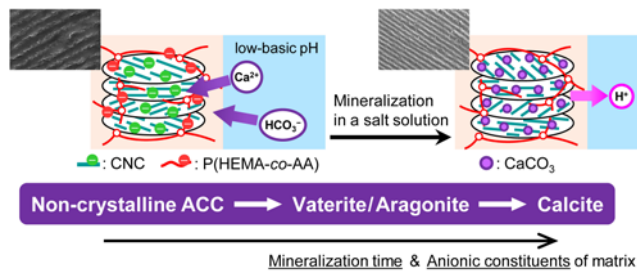
Highlights:

CaCO$_3$ mineralization was conducted using CNC/polymer composite films invested with a chiral nematic order.

Both the CNC and the acrylic acid unit constituting the polymer contributed to facilitate CaCO$_3$ deposition inside the film matrix.

The polymorph of the deposited carbonates was variable depending on the matrix composition.

The mineralized films retained the chiral nematic arrangement, but the helical pitch was reduced.

Heat/flame resistance of the CNC/polymer films was markedly improved by the CaCO$_3$ deposition.